Toward MRI and Optical Detection of Zwitterionic Neurotransmitters: Near-Infrared Luminescent and Magnetic Properties of Macrocyclic Lanthanide(III) Complexes Appended with a Crown Ether and a Benzophenone Chromophore

Fatima Oukhatar, Svetlana Eliseeva, Celia Bonnet, Matteo Placidi, Nikos Logothetis, Stéphane Petoud, Goran Angelovski, Éva Tóth

Towards MRI and Optical Detection of Zwitterionic Neurotransmitters: Near-Infrared Luminescent and Magnetic Properties of Macrocyclic Lanthanide(III) Complexes Appended with a Crown Ether and a Benzophenone Chromophore

Fatima Oukhatar,[†§] Svetlana V. Eliseeva,[†] Célia S. Bonnet,[†] Matteo Placidi,[§] Nikos K. Logothetis, [§₸] Stéphane Petoud,[*†] Goran Angelovski[*§] and Éva Tóth[*†]

[†] Centre de Biophysique Moléculaire, CNRS UPR 4301, Université d'Orléans, rue Charles Sadron, 45071 Orléans, Cedex 2, France.
[§] Department of Physiology of Cognitive Processes and MR Neuroimaging Agents, Max Planck Institute for Biological Cybernetics, Max-Planck-Ring 8, 72076 Tubingen, Germany.
[₸] Department of Imaging Science and Biomedical Engineering, University of Manchester, Manchester, UK.

* E-mail: eva.jakabtoth@cnrs-orleans.fr
* E-Mail: goran.angelovski@tuebingen.mpg.de
* E-mail: stephane.petoud@inserm.fr

KEYWORDS. Magnetic resonance imaging, luminescence, near-infrared, bimodal agents, lanthanide complexes, neurotransmitters, benzophenone, human serum albumin.

ABSTRACT

Thanks to their versatile magnetic and luminescence features, lanthanide complexes have gained a central position in biomedical imaging as MRI contrast agents and optical imaging probes. In addition, appropriate chemical design allows the modification of the magnetic relaxation properties of Gd^{3+} complexes and the optical properties of visible or near-infrared emitting lanthanide chelates upon interaction with various biomarkers, which makes them ideal candidates for the creation of responsive agents. In this Forum article, we demonstrate such design principles as well as the difficulties encountered in the context of neurotransmitter detection. Lanthanide(III) complexes of a macrocyclic ligand incorporating a benzophenone chromophore and a monoaza-crown ether (**LnL^3**) have been synthesized as responsive probes to monitor amino acid neurotransmitters either in magnetic resonance imaging (Ln=Gd) or in near-infrared optical detection (Ln=Nd or Yb). The parameters characterizing the water exchange and the rotational dynamics of the Gd^{III} complex were assessed by ^{17}O NMR and ^{1}H NMRD. In the presence of zwitterionic neurotransmitters, the inner sphere water molecule is replaced by the carboxylate function of the neurotransmitters in the Gd^{III} complex, leading to a decrease of the longitudinal relaxivity from 6.7 $mM^{-1}s^{-1}$ to 2-2.5 $mM^{-1}s^{-1}$ (300 MHz and 37 °C). Apparent affinity constants range from K_a = 35 for γ-aminobutyric acid (GABA) to 80 M^{-1} for glycine and glutamate, and there is no selectivity with respect to hydrogen-carbonate (K_a = 232; pH 7.4). The Gd^{III} complex interacts with human serum albumin (HSA) resulting in a 60% increase in relaxivity (20 MHz, 37 °C) in the absence of neurotransmitters. The HSA-bound complex, however, revealed to be less responsive to neurotransmitters due to the displacement of the Gd^{III}-bound water by HSA, which was confirmed by the hydration number calculated from luminescence lifetimes of the HSA-bound Eu^{III} complex.

The creation of an imaging agent suitable for near-infrared (NIR) detection of neurotransmitters for an enhanced sensitivity in biological systems using the benzophenone moiety as sensitizer of lanthanide luminescence was also attempted. Upon excitation at 300 nm of the benzophenone chromophore in aqueous solutions of Nd**L^3** and Yb**L^3**, characteristic near-infrared emissions of Nd^{III} and Yb^{III} were observed due to $^4F_{3/2} \rightarrow {}^4I_J$ (J = 9/2 – 13/2) and $^2F_{5/2} \rightarrow {}^2F_{7/2}$ transitions, respectively, indicating that this chromophore is a suitable antenna. Despite these promising results, luminescence titrations of Nd^{3+} and Yb^{3+} complexes with neurotransmitters were not conclusive due to a chemical conversion of the ligand triggered by light, preventing quantitative

analysis. The observed photochemical reaction of the ligand is strongly dependent on the nature of the lanthanide chelated; it is considerably slowed down in the presence of Nd^{III} and Eu^{III}.

INTRODUCTION

Responsive magnetic resonance imaging (MRI) agents act as reporters of the biological environment where they are distributed by generating an MRI signal dependent on tissue parameters such as pH, concentration of endogeneous ions, enzymes, etc.[1] Combining MRI detection with complementary imaging techniques can provide additional, less ambiguous information. Multimodal approaches are becoming more common in both biomedical research and clinical imaging, and the development of responsive imaging agents with detection capabilities has recently triggered increasing interest.[2-4] Lanthanide(III) ions (Ln^{III}) have versatile magnetic and luminescent properties and in the past, we and others have explored approaches for the creation of bimodal imaging agents adapted for combined MRI and optical detection.[5-7] While the Gd^{III} ion with its S=7/2 electron spin and slow electronic relaxation is the most efficient relaxation agent among all paramagnetic metal ions, the luminescence properties of several lanthanides of different natures offer complementary advantages over organic dyes.[8] Their emission bands are much narrower and cover UV, visible and near-infrared (NIR) spectral ranges. Ln^{III} exhibit long luminescence lifetimes (from μs up to ms) thus enabling time-gated detection. Nevertheless, due to the Laporte forbidden nature of most of the f-f transitions of lanthanide(III) ions, they are characterized by very low absorption coefficients (< 10 M^{-1} cm^{-1}) that makes their direct excitation inefficient reducing therefore the number of emitted photons. This problem can be circumvented by locating in sufficiently close proximity Ln^{III} ions and chromophoric moieties able to absorb the excitation light and transfer the resulting energy to the Ln^{III} ("antenna effect").[9]

The detection of neurotransmitters (NT) has been in the focus of recent efforts in molecular MRI.[10] Direct monitoring of neural activity by MRI *via* the detection of appropriate biomarkers is one of the current challenges in neuroimaging. One strategy involves engineered proteins obtained in directed evolution. In several mutation rounds, the affinity of paramagnetic metalloproteins could be tuned for monoamine NT and these probes have been used in small animal studies to detect dopamine or serotonin release.[11-12] In a different approach based on artificial NT receptors, we have reported a series of MRI contrast agents that are responsive to zwitterionic NTs including

the ligands $\mathbf{L}^1$ and $\mathbf{L}^2$ (Scheme 1).[13-14] They consist of conjugates of Gd^{III} DO3A-type chelates and eighteen-membered mono- or triaza-crown ethers. These complexes act as ditopic receptors that can accommodate zwitterionic, amino acid NTs in a dual binding mode. The binding occurs between the positively charged Ln^{III} chelate and the carboxylate function of the NTs, and between the azacrown ether and the amine group of the neurotransmitters. The MRI response of the Gd^{III} probe is based on the displacement of the inner-sphere water molecule(s) upon neurotransmitter binding.

Several optical approaches have been also developed to sense neurotransmitters, involving both small molecule and genetically encoded protein sensors,[15] but none of them was based on lanthanide luminescence. In our previous studies, the interaction with the selected neurotransmitters has been demonstrated to impact also the optical properties of the Eu^{III} and Tb^{III} complexes of the ligand $\mathbf{L^1}$ and $\mathbf{L^2}$;[14] however, the phenyl group proved to be a poor sensitizer of these luminescent Ln^{III} ions. The luminescence of NIR emitting lanthanide cations is attractive in respect to visible ones for application in biological systems as these possess only a low native fluorescence in the NIR spectral range.[16] This advantage allows to obtain a better signal to noise ratio and an enhanced detection sensitivity. Our goal here was to design a new chemical structure by introducing a suitable lanthanide chromophoric sensitizer to generate an antenna effect[9] in the ligand structure in order to develop a neurotransmitter-sensitive probe that would provide detection capabilities both in MRI and optical imaging in the NIR domain, depending on the coordinated Ln^{III} ion. Y. Shiraishi et al.,[17] and J.A. Gareth Williams[18,19] et al. reported the sensitization of characteristic emission of Eu^{III} and Tb^{III} ions in the visible range *via* the benzophenone (BP) moeity. In addition, it has been found that Eu^{III} complexes with the *para*-substituted BP derivative exhibit significantly higher luminescence quantum yields compared to the corresponding *ortho*- and *meta*-substituted complexes.[19] S. Pope et al. have also demonstrated the sensitization of characteristic Nd^{III} emission in the NIR range in a ternary cyclen complex with benzoylbenzoate.[20] The main electronic features of BP chromophores involve the n,π* character of the excited triplet state and quantitative intersystem crossing efficiency with quantum yields for the formation of the triplet state close to unity. Therefore, the BP chromophore has been incorporated in the Ln^{III} chelate which also bears a mono-aza crown ether as illustrated in Scheme 1 (ligand $\mathbf{L}^3$).

In addition, benzophenone is known to bind proteins such as HSA *via* hydrophobic interactions.[21] HSA-binding of the Gd**L**^{3} complex can lead to higher proton relaxivities due to a substantial increase of the inner sphere contribution to the relaxivity. Since the interaction of Gd**L**^{3} with zwitterionic NTs is expected to reduce the hydration number thus eliminating the inner sphere contribution to relaxivity, we hypothesized that protein binding could contribute to achieve a more important relaxivity change and lead to a more sensitive detection of neurotransmitters.

In this work, we therefore attempted to explore the potential of Ln^{III} complexes appended with both the azacrown ether and the chromophore for sensing neurotransmitters by means of dual modal imaging. Given the previously shown ability of such Gd^{III} complexes to affect the relaxation time of water in the presence of amino acid neurotransmitters and follow their flux *ex vivo*,[13] an expansion of their scope to additional imaging modalities would be very advantageous for investigating neuronal signaling. The advantage of our approach consists of using identical chelators and their coordination properties in interaction with the guest molecules (i.e. neurotransmitters), while swapping only the Ln^{III} ion and hence the paramagnetic or luminescence emission properties of the whole system.

In general, the combination of MRI and *in vivo* NIR optical imaging using bimodal responsive agents can further advance molecular imaging towards more specific and powerful detection of biomarkers.[22] MRI also provides a morphological background image in addition to the molecular imaging acquired by using a responsive MRI probe. When injecting a cocktail of the MRI and the optical probe, their individual concentration can be easily adjusted to the sensivity of each technique (several orders of magnitude higher for optical than for MRI detection). The complexes formed with Gd^{3+} or with a luminescent lanthanide will have essentially identical biodistribution, given the very similar chemical properties of lanthanide ions. Simultaneous, bimodal MRI and optical detection can be useful and easily achieved for *ex vivo* tissue imaging for instance.[13] Concerning *in vivo* studies, in a simple, sequential experimental set-up, *in vivo* MRI can be realized first, while optical detection can be used for subsequent post mortem histology. Finally, both MRI and optical imaging can be realized *in vivo*. In this case, overlapping the morphological and molecular MR images with an *in vivo* NIR optical image relying on a probe whose signal is similarly dependent on the same biomarker renders the detection less ambiguous.

To this end, we investigated chelator $\mathbf{L}^3$ and its Ln$\mathbf{L}^3$ complexes (Ln=Gd, Eu, Yb, Nd), exploring their relaxometric and optical properties in buffered media and upon interaction with neurotransmitters. In specific, we assessed the relaxivity features, including the parameters that describe water exchange, rotational dynamics and relaxation efficacy on the Gd^{III} complex formed with ligand $\mathbf{L}^3$. The photophysical properties of NIR-emitting Yb^{III} and Nd^{III} derivatives have been investigated. The effect of neurotransmitters on relaxometric properties of Ln$\mathbf{L}^3$ complexes has been analyzed. We have assessed HSA binding of Gd$\mathbf{L}^3$ and carried out relaxometric titrations with neurotransmitters in the presence of the protein.

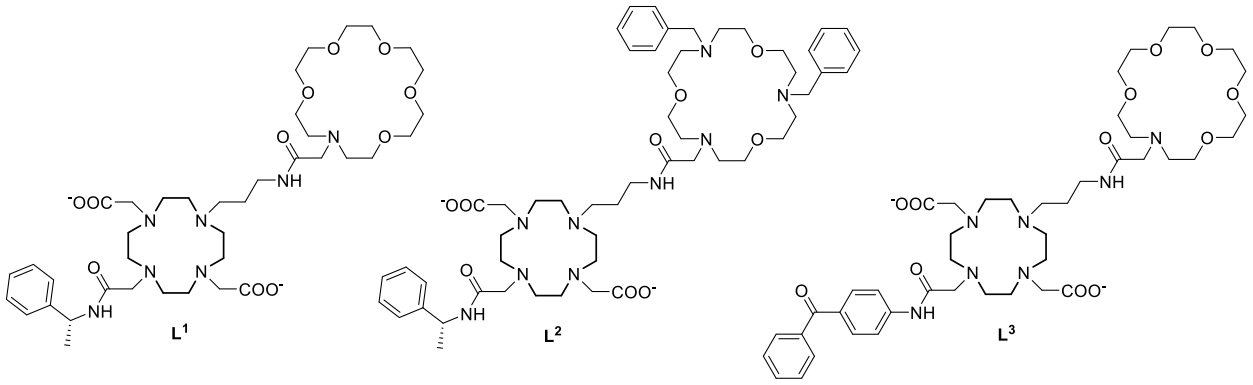

Scheme 1: Structure of the benzophenone-containing ligand $\mathbf{L}^3$. Ligands $\mathbf{L}^1$ and $\mathbf{L}^2$ have been described previously and are shown here for comparison.[14]

Results and discussion

Synthesis of the ligand $\mathbf{L}^3$:

Para-benzophenone-chloroacetamide was prepared from the commercially available 2-aminobenzophenone by acetylation with chloroacetyl chloride.[23] It was used for mono-N-functionalization of *t*Bu-DO2A to yield the intermediate **1** (Scheme 2). Functionalization of the fourth NH group located in the cyclen ring *via* a reductive amination with N-Cbz protected 3-aminopropanal afforded **2**, followed by the removal of the Cbz protecting group to give the amine **3**. This amine was coupled with monoaza-crown carboxylic acid **4** [14] using HBTU as coupling agent to result in the compound **5**. Finally, the acid hydrolysis of *tert*-butyl esters resulted in the ligand $\mathbf{L}^3$.

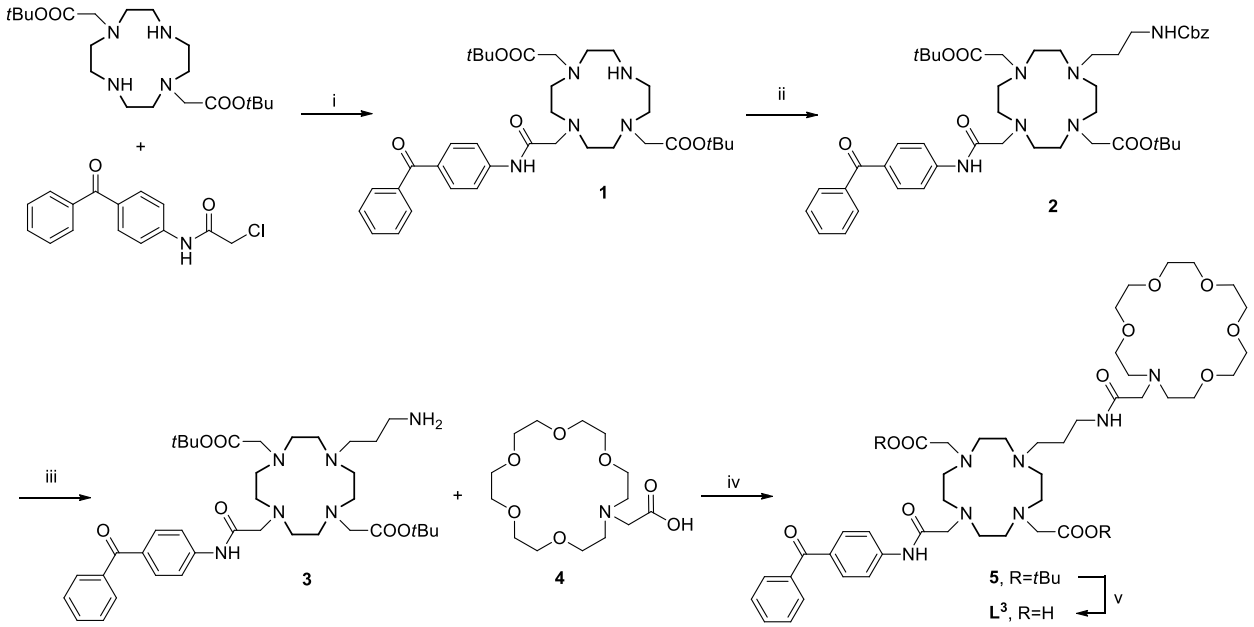

Scheme 2. Synthetic pathway to ligand $\mathbf{L}^3$. i) H_2O:dioxane, pH7-8.5; ii) $OHC(CH_2)_3NHCbz$, $Na(OAc)_3BH$, THF; iii) H_2, 10% Pd/C, EtOH; iv) HBTU, DMF, r.t.; v) HCO_2H, 60 °C.

^{17}O NMR and NMRD study on the Gd^{III} complex

In order to assess the parameters describing water exchange and rotational dynamics on $Gd\mathbf{L}^3$, a variable temperature ^{17}O NMR study was performed on aqueous solution of this Gd^{III} complex. Figure 1 shows the temperature dependency of the reduced ^{17}O chemical shifts ($\Delta\omega_r$), and transverse ($1/T_{2r}$) and longitudinal ($1/T_{1r}$) relaxation rates. Above ~310 K, the transverse ^{17}O relaxation rates, $1/T_{2r}$, increase with decreasing temperature, indicating here that the complex is in the fast exchange regime. At lower temperatures, the transverse relaxation rates turn into a slow exchange regime. The reduced chemical shifts follow the same trend.

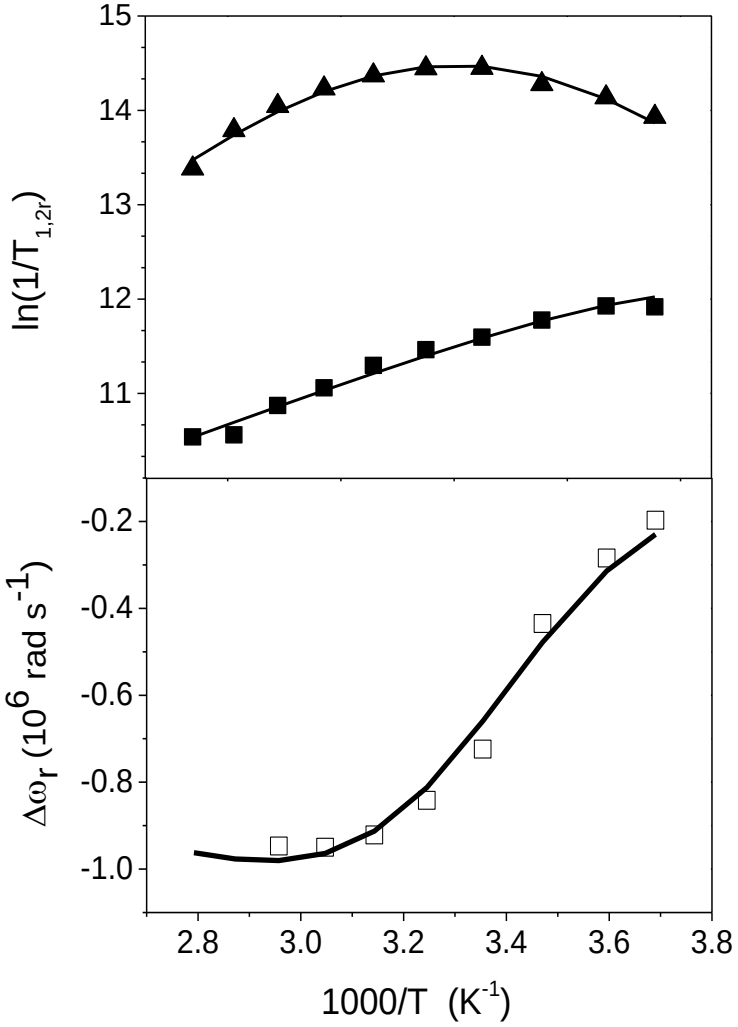

Figure 1: Temperature dependence of the reduced transverse ^{17}O relaxation rates, $1/T_{2r}$ (▲), $1/T_{1r}$ (■) and the reduced ^{17}O chemical shifts, $\Delta\omega_r$ (□)) for Gd**L**^{3}. The curves represent the fit to the experimental data.

Transverse ^{17}O relaxation is governed by the scalar relaxation mechanism, thus contains no information on the rotational motion of the system. While in the slow exchange regime, the reduced transverse relaxation rates are directly determined by the water exchange rate, in the fast exchange regime, they are defined by the transverse relaxation rate of the bound water oxygen, $1/T_{2m}$, itself influenced by the water exchange rate, k_{ex}, the longitudinal electronic relaxation rate, $1/T_{1e}$, and the scalar coupling constant, $A/\hbar$. In contrast to $1/T_{2r}$, the longitudinal ^{17}O relaxation rates, $1/T_{1r,}$ are determined by dipole-dipole and quadrupolar relaxation mechanisms, both related to rotation. The dipolar term depends on the Gd^{3+}-water oxygen distance, r_{GdO}, while the quadrupolar term is influenced by the quadrupolar coupling constant, $\eta(1+\eta^2/3)^{1/2}$. Finally, the ^{17}O

chemical shifts give a direct indication of the hydration state of the complex and the reduced chemical shifts are determined by $A/\hbar$.

In order to get more insight into the parameters involved in the paramagnetic relaxation pathway, we have also measured NMRD profiles in a 1.0 mM Gd**L**^{3} solution over an extended range of frequencies (0.01 – 400 MHz) at 25°C and 37°C (Figure 2). A well-defined relaxivity hump is observed at 40-80 MHz which is characteristic of slow tumbling. This relaxivity hump is much more accentuated than in the case of Gd**L**^{1} [14] which indicates slower rotation for Gd**L**^{3} compared to Gd**L**^{1}. This is also in accordance with the experimental longitudinal ^{17}O relaxation rates which are higher for Gd**L**^{3} than for Gd**L**^{1} (Fig. 1 and ref. [14]). A concentration-dependent relaxometric study in the range 0.05–7.5 mM showed increasing relaxivities upon increasing the concentration (Figure S1, Supporting Information), evidencing aggregation of Gd**L**^{3} in aqueous solution. Therefore, given the different concentration in the ^{17}O NMR (21.5 mmol/kg) and NMRD samples (1 mM), the ^{17}O NMR and NMRD data have been analysed separately according to the Solomon-Bloembergen-Morgan theory for the inner sphere relaxation and the Freed model for the outer sphere term.[24] Details of the analysis and the equations used in the fit are given in the Supporting Information, and the most important parameters obtained are listed in Table 1. In the fit of the proton relaxivities, the water exchange parameters were fixed to values obtained in the ^{17}O NMR study. The rotational dynamics could be only described by applying the Lipari-Szabo approach that separates local and global motions, characterized by the local and global rotational correlation times, τ_{lH}^{298} and τ_{gH}^{298}, respectively, and a model independent order parameter, S^2. We should note that the Lipari-Szabo approach is not applicable to the analysis of the ^{17}O $1/T_1$ data since they have been measured at a single magnetic field.

Table 1: Parameters obtained from the fitting of the transverse and longitudinal ^{17}O NMR relaxation rates and chemical shifts as a function of temperature at 11.7 T. The analogous parameters for Gd**L**^{1} and GdDOTA are also shown for comparison.

	Gd**L**^{3}	Gd**L**^{1a}	GdDOTA[e]
q	1	1	1
k_{ex}^{298} (10^6s^{-1})	6.7±0.4	13.0	4.1

$\Delta H^{\neq}$ (kJ.mol^{-1})	34.8± 0.3	33.3	49.8
$\Delta S^{\neq}$ (J.mol^{-1}K^{-1})	+3±1	+4	+48.5
τ_{RO}^{298}(ps)	681±3	292	90,[b] 77[c]
τ_{gH}^{298}(ps)[d]	650±40		
τ_{lH}^{298}(ps)[d]	70±8		
S^{2} [d]	0.22±0.01		
E_R (kJ.mol^{-1})	16.4±0.4	17.6	16.1
τ_v^{298}(ps)	3.8±0.8	2.0	11
Δ^2(10^{20}s^{-1})	0.8±0.1	0.36	0.16
A/ħ(10^6rad.s^{-1})	- 3.8±0.3	- 3.7	-3.7
C_{os}	0.1	0.21	0.21

a From reference [14]. b Rotational correlation time of the Gd–O_{water} vector, from ^{17}O $1/T_{1r}$ data. c Rotational correlation time of the Gd–H_{water} vector, from NMRD data. d global (τ_{gH}^{298}) and local (τ_{lH}^{298}) rotational correlation times and order parameter (S^2) obtained from the fit of NMRD data using the Lipari-Szabo approach (E_l and E_g fixed to 20 kJ/mol). e From reference [25]

For Gd**L**^{3}, partially in the fast water exchange regime, the reduced chemical shifts and, consequently the calculated scalar coupling constant, provide a direct indication on the monohydrated nature of the complex, analogously to Gd**L**$^{\mathbf{1}}$ and Gd**L**$^{\mathbf{2}}$. In order to confirm the hydration number q = 1, luminescence lifetime measurements have been carried out on the Eu^{III} analogue. The experimental luminescence decays could be best fitted by a biexponential function involving two main components with τ_1 = 397 µs (63%) and τ_2 = 852 µs (37%) in HEPES buffered H_2O, and by a monoexponential function in D_2O, yielding τ = 1492 µs (Figure S2, Supporting Information). The biexponential character of the decay could result from the presence of two differently hydrated species, and based on the lifetime values, one can calculate using empirical equations[26-27] q_1 = 1.7 and q_2 = 0.1 suggesting a bishydrated and a non-hydrated complex in solution. The presence of equilibrium between such differently hydrated complexes is rather improbable. On the other hand, for a hydration equilibrium between q = 0 and q = 2 species, one would expect a strong temperature dependence shifting the equilibrium towards the non-hydrated

complex at high temperatures, as previously observed.[28] This should be visible on the experimentally measured ^{17}O chemical shifts, leading to a strong decrease of the values at higher temperatures. As such an anomaly in the chemical shifts is definitively not observed, we conclude that the hydration number is one as it is unambiguously determined by the chemical shifts and the biexponential nature of the luminescence decay is not originating from the presence of two so differently hydrated species. It should be noted that the estimation of hydration numbers from luminescence lifetime values in water and in deuterated water rely on the phenomenological equations.[26-27] Their use, however, is restricted by a number of assumptions, in particular, that the quenching by solvent vibrations is the main deactivation process and that all the other non-radiative paths are the same in H_2O and D_2O. Nevertheless, these points might not be always satisfied in a particular system leading to erroneous calculation and corresponding values of coordinated solvent molecules.

The water exchange rate on Gd**L**^{3} is increased with respect to GdDOTA, although this increase is much more limited when compared to Gd**L**$^{\mathbf{1}}$. We have previously related the fast water exchange for Gd**L**$^{\mathbf{1}}$ [14] to the metal coordination of the amide oxygen of the linker between the crown ether and the macrocycle which induces considerable constraint around the water binding site. A higher steric constraint is known to favour the leaving of the coordinated water in the exchange process.[29] Although the water exchange mechanism has not been directly assessed (it would be possible *via* variable pressure measurements, but beyond the scope of this study), the activation entropy calculated gives a rough indication for an interchange mechanism for both Gd**L**$^{\mathbf{3}}$ and Gd**L**$^{\mathbf{1}}$**.** This implies that the incoming water molecule plays also a role in the water exchange. The steric demand of the bulkier benzophenone group can strongly limit the approach of the incoming water to the binding site and lead to a decrease of the water exchange rate with respect to Gd**L**^{1}.
The rotational correlation time obtained in the fit of the longitudinal ^{17}O relaxation rates is long in comparison with that of GdDOTA or Gd**L**^{1}, which clearly reflects the aggregation. This aggregation phenomenon is not surprising given the low solubility of benzophenone in water.

The ^1H relaxivity of Gd**L**$^{\mathbf{3}}$ is 9.0 $mM^{-1}s^{-1}$ at 298 K and 20 MHz (1 mM). This value is larger than that for the analogous Gd**L**$^{\mathbf{1}}$ complex (r_1=8.3 $mM^{-1}s^{-1}$) to which one inner sphere water molecule was also assigned. When compared to typical q=1 complexes such as GdDOTA (r_1=4.7 $mM^{-1}s^{-}$

[1]),[28] the relaxivity of Gd**L**^{3} is impressive at intermediate frequencies (20-80 MHz) and can be clearly accounted for by the significantly longer rotational correlation time due to the bigger molecular size and to partial aggregation which already occurs at 1 mM concentration. Such high relaxivity can be advantageous for sensing applications which are based on variation of the hydration number of the Gd^{III} complex upon interaction with the biomarker. Indeed, the contribution of the inner sphere relaxation mechanism to the overall relaxivity is maximized for slowly rotating systems, consequently, the relaxivity change observed at intermediate frequencies upon replacement of the hydration water will be more substantial.

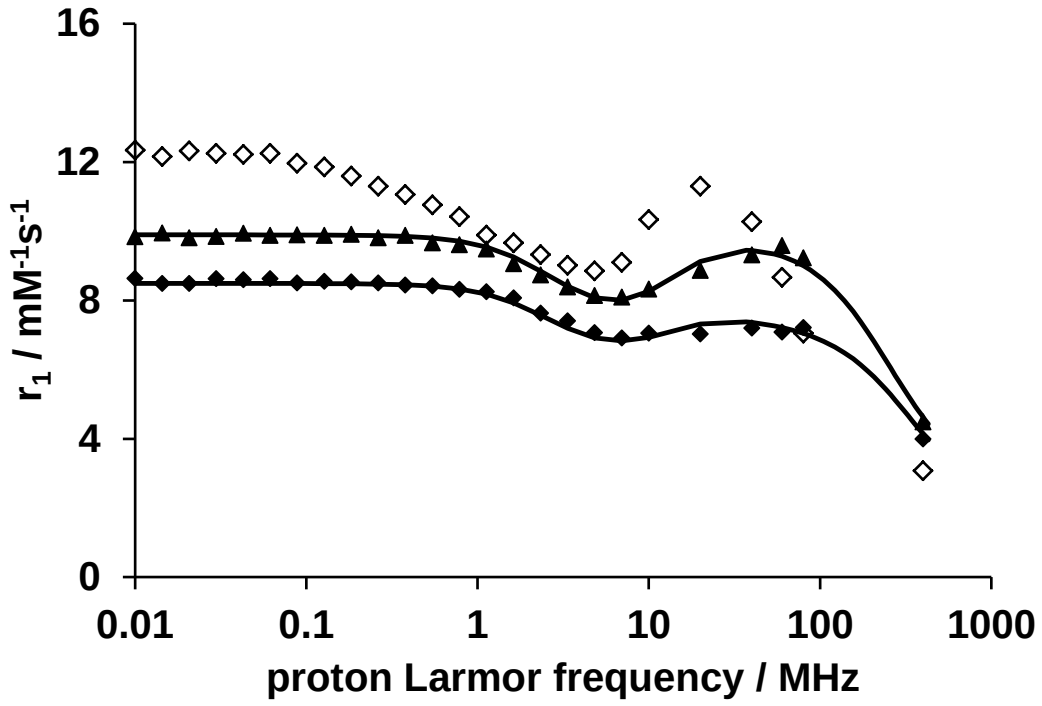

Figure 2. Proton relaxivities, r_1, of 1 mM aqueous solution of Gd**L**^{3} in HEPES (25 mM, pH7.4), as a function of the Larmor frequency in the absence of the human serum albumin (HSA) at 25°C (▲) and 37°C (■) and in presence of 0.6 mM HSA at 37°C (◊), after subtraction of the diamagnetic contribution of HSA.

Binding of GdL^{3} to HSA

Since it was established that the relaxivity of a Gd^{III} complex can be strongly enhanced by formation of non-covalent adducts with slowly rotating macromolecules, increasing attention has

been focused to create MRI agents with high binding affinity to human serum albumin (HSA).[30] HSA is the most abundant protein in plasma and has two distinct sites for high-affinity binding of a broad spectrum of endogenous substances such as long chain fatty acids, thyroid hormones, etc.[31] The plasma concentration of HSA is around 0.6 mM and a high HSA-binding ability allows long-term retention of the agent in the intravascular space. Hydrophobic residues have been typically used to promote the binding between MRI contrast agents and HSA.[32] Benzophenone has been reported to bind HSA with an association constant of $K_a = 8.5\times10^4$ M^{-1}, as determined by spectroscopic methods.[33] On this basis, binding to HSA was investigated by titrating a solution of Gd**L**$^{\mathbf{3}}$ (0.1 mM, 25 mM HEPES buffer) with HSA (Figure 3). The affinity constant for the ternary complex Gd**L**$^{\mathbf{3}}$-HSA was estimated from this titration to be $K_a = 8.7\times10^4$ M^{-1}, assuming a single binding site. Nevertheless, HSA has potentially more than one binding sites.[34] We also performed a fit by discarding the first points of the titration curve which are below 1:1 HSA/Gd**L**$^{\mathbf{3}}$ ratio. With this approach, provided there are several binding sites, we focus only on the strongest one. In this case, the quality of the fit was somewhat better while the affinity constant calculated, $K_a = 4.0\times10^4$ M^{-1}, is of the same order of magnitude as the previous one (Figure S3, Supporting Information). In any case, the binding affinity of Gd**L**$^{\mathbf{3}}$ is comparable to that of benzophenone alone.

The relaxivity of Gd**L**$^{\mathbf{3}}$ in the presence of 0.6 mM HSA has been also recorded at variable magnetic fields (0.01-9.4T) (Figure 2). The non-covalent interaction of Gd**L**$^{\mathbf{3}}$ with HSA leads to a 60% increase of the relaxivity (r_1 = 11.62 $mM^{-1}s^{-1}$ at 37°C, 20 MHz, 1 mM Gd**L**$^{\mathbf{3}}$ and 0.6 mM HSA) and as expected, a relaxivity peak centered at 20 MHz is observed in the NMRD profile, due to the slower rotation of the protein bound complex. Under the conditions of 1 mM Gd**L**$^{\mathbf{3}}$ and 0.6 mM HSA and based on the binding constant determined above, $K_a = 8.7\times10^4$ M^{-1}, 59% of Gd**L**$^{\mathbf{3}}$ is estimated to be bound to the protein (it would be 57% if calculated with $K_a = 4.0\times10^4$ M^{-1}). The relaxivity calculated for this bound species is 14.5 $mM^{-1}s^{-1}$, a value which is rather modest for a macromolecular agent. In comparison, for MS-325 $r_1 \sim 45$ $mM^{-1}s^{-1}$ was reported under similar conditions.[34] In order to understand the reasons for this behaviour, we have assessed the hydration number, q, of the corresponding Eu**L**$^{\mathbf{3}}$ complex in the presence of HSA (c_{EuL3} = 1 μM, HSA = 0.6 mM) by measuring luminescence lifetimes. The q value determined under these conditions is 0.1±0.2, indicating the replacement of the inner-sphere water molecule of Gd**L**$^{\mathbf{3}}$ by the amino acid side chain residues of the HSA. Such diminution of the hydration number upon protein (HSA) binding has been observed for other DO3A-derivative Gd^{3+} complexes[32] and has been

experimentally evidenced by ENDOR measurements that allow direct assessment of the hydration number.[35] The small relaxivity increase observed in the presence of HSA might originate then from second sphere water molecules and from a small quantity of residual hydration water in the HSA-bound complex. Consequently, we can conclude that the binding of free carboxylate functions in the side chains of HSA to the Gd^{III} also participates to the Gd**L**^{3} – protein interaction and contributes to the affinity.

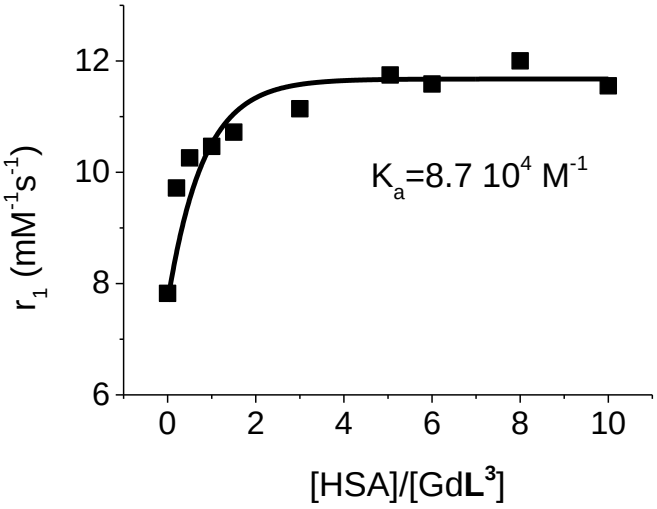

Figure 3. Plot of the longitudinal water proton relaxation rate of a 0.1 mM Gd**L**^{3} solution in HEPES (25mM, pH 7.4) as a function of HSA concentration at 20 MHz and 37°C.

Binding studies of LnL^{3} with neurotransmitters

Relaxometric titrations of Gd**L**^{3} were undertaken at 300 MHz and 37°C to measure the change of r_1 as a function of added neurotransmitters and HCO_3^-. The relaxivity of Gd**L**^{3} is 6.7 $mM^{-1}s^{-1}$ at 300 MHz and 37°C, in comparison to 7.8 $mM^{-1}s^{-1}$ at the same magnetic field and temperature for Gd**L**^{1}. Figure 4 depicts the relaxometric titration curves of Gd**L**^{3} with acetylcholine, GABA, aspartate, glutamate, glycine and hydrogen-carbonate. The titration curves were fitted to obtain affinity constants for the ternary complexes (K_a=[GdL–A]/[GdL][A], in which A stands for the analyte amino acid NT or anion). The fitted values of the affinity constants are reported in Table 2.

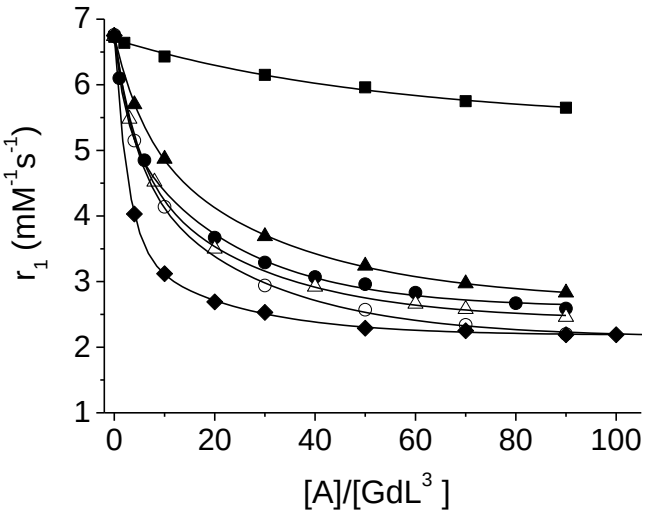

Figure 4. ^{1}H NMR relaxometric titrations of Gd**L**^{3} with Acetylcholine (filled squares,■), GABA (filled up-triangles,▲), Aspartate (filled circles, ●), Glutamate (open triangles, Δ), Glycine (open circles, ○), and hydrogen carbonate (filled diamonds, ♦) at 300 MHz in D_2O, 37 °C and pH 7.4 (HEPES 25mM).

Table 2: Affinity constants and percentages of the observed relaxivity change upon interaction of Gd**L**^{3} with neurotransmitters and HCO_3^-, at 300MHz and 37 °C (HEPES 25 mM, pH 7.4). Data for Gd**L**^{1} are shown for comparison.

	GdL^1 [a]		**GdL^2** [c]		**GdL^3**	
	K_a (M^{-1})	$-\Delta r_{1p}$(%)	K_a (M^{-1})	$-\Delta r_{1p}$(%)	K_a (M^{-1})	$-\Delta r_{1p}$ (%)
Glycine	178	74[a]	345	81	81	75
Glutamate	110	69	312	77	81	70
GABA	125[b]	67[b]	99	72	35	70
Aspartate	-	-	345	76	71	67
HCO_3^{2-}	-	-	440	74	232	69
HPO_4^-	0	0	0	0	-	12
Acetylcholine	-	30	-	32	-	16

[a] From reference [14]. [b] Values obtained from titrations in H_2O at 60 MHz. [c] From reference [13]

The relaxometric titration curves and the resulting data shown in Table 2 reveal some apparent trends for Gd**L**^{3}: similarly to Gd**L**^{1} and Gd**L**^{2}, the binding of the γ-amino acid GABA is weaker than that of α-amino acid neurotransmitters, while acethylcholine binds to a much lesser extent. Gd**L**^{3} also displays a high affinity towards HCO_3^-.[13-14] In contrast to Gd**L**^{1} or Gd**L**^{2}, the binding affinity of Gd**L**^{3} towards the zwitterionic neurotransmitters has decreased considerably (though the overall decrease of relaxivity on binding did not change). Therefore, it can be concluded that the introduction of the BP moiety leads to a loss of selectivity for neurotransmitters over carbonate. Additionally, there is also a small change in relaxivity induced by hydrogen phosphate in the case of Gd**L**^{3} (Table 2), while Gd**L**^{1} was insensitive to the presence of this ion. This change is insignificant when compared to the response to the other neurotransmitters.

In the mammalian central nervous system, glutamate is the major excitatory neurotransmitter. Although its extracellular concentration in brain fluids is low (typically in the micromolar range), synaptically released glutamate concentrations can reach few millimolar,[36] which can be well adapted for MRI detection (glutamate concentration inside neurons of the brain is also between 1 and 10 mM). To detect such concentrations, affinity constants of the MRI sensor for the neurotransmitter should be around 10^3 M^{-1}, close to the values determined for Gd**L**^{3}.

We also carried out a similar titration experiment of the complex with glutamate in a 0.6 mM HSA solution (1 mM Gd**L**^{3}, 37°C, 20 MHz; Figure 5). Upon addition of glutamate, the relaxivity drops from 11.54 $mM^{-1}s^{-1}$ to 6.57 $mM^{-1}s^{-1}$. An apparent binding constant to glutamate, in the presence of HSA, can be estimated by fitting the titration curve in Figure 5. The affinity constant drops from 81 M^{-1} in the absence to 14.8 M^{-1} in the presence of HSA. Consequently, the relaxivity decrease is originating partly from glutamate interaction with the non-HSA-bound complex, which is present in 41 % (according to the affinity constant, see above). In addition, when present in a large excess, glutamate becomes a competitor of HSA and will replace the protein carboxylates in the coordination sphere of the metal in Gd**L**^{3}, further contributing to the overall relaxivity decrease.

In overall, the Gd**L**^{3} system exhibits interesting relaxometric changes upon interaction with neurotransmitters. Its relaxivity is diminished in the presence of selected amino acid neurotransmitters, to a similar extent as observed for previously reported analogues.[13-14] In the presence of human serum albumin, the relaxivity increases at intermediate fields due to slower rotation; however, this relaxivity gain is limited by a decrease in the Gd^{III} hydration number. In

consequence, the neurotransmitter-sensing ability of the complex is partially preserved but not improved in the presence of HSA.

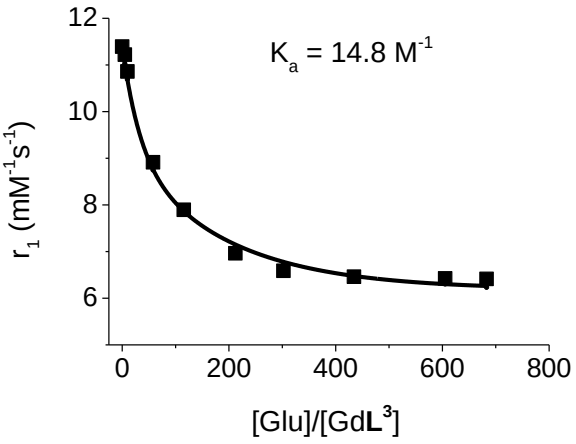

Figure 5. Relaxivity profile of 1 mM Gd**L**^{3} in response to addition of glutamate in the presence of 0.6 mM HSA in HEPES (25 mM, pH 7.4) at 37°C and 20 MHz.

Photophysical properties

Ligand-centered properties.

In the absorption spectrum of the ligand **L**^{3}, we can observe the presence of two broad overlapping bands with apparent maxima at 260 nm (ε_{260} = 25 370 $M^{-1}cm^{-1}$) and 300 nm (ε_{300} = 33 990 $M^{-1}cm^{-1}$). They are assigned to π*←π transitions on the basis of their large extinction coefficients (Figure 6). In addition, a broad band attributed to π*←n transitions with significantly lower molar absorptivity is present at longer wavelengths (ε_{390} = 1610 $M^{-1}cm^{-1}$). Absorption spectra of Gd^{III}, Yb^{III} and Nd^{III} complexes formed with the ligand **L**^{3} are similar and exhibit broad bands in the range 240–350 nm centered at 290 nm (ε_{290} = 37 400–37 500 M^{-1} cm^{-1}) and corresponding to π*←π transitions. π*←n transitions could not be detected (Figure 6). It should be noted here that absorption bands of **L**^{3} and Ln**L**^{3} are similar to those observed previously for cyclen compounds appended with *para*-substituted benzophenones.[18-19, 37]

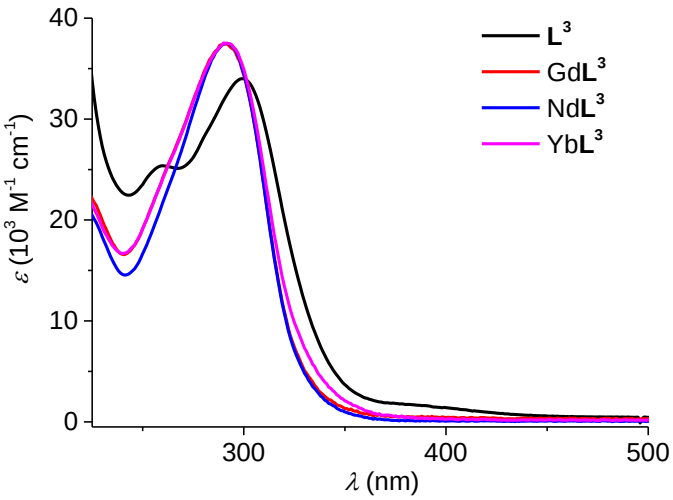

Figure 6. Absorption spectra of Ln**L**^{3} (Ln = Yb^{III}, Gd^{III} and Nd^{III}; 100 µM in 25 mM HEPES buffer, pH = 7.4, room temperature).

In order to assess the energy position of the triplet state of **L**^{3}, the phosphorescence spectrum of the Gd**L**^{3} complex was recorded upon excitation at 300 nm with the application of a delay after the excitation flash of 50 µs (Figure S4). Indeed, no energy transfer can occur from the BP chromophore to the $^{6}P_{7/2}$ level of the Gd^{III} ion because of its too high energy (32 000 cm^{-1}) making possible the observation of the pure ligand-centered emission. The phosphorescence spectrum of the Gd**L**^{3} complex exhibits a broad band emission with a strong vibrational progression in the range of 400–620 nm with an apparent maximum at 452 nm. The energy position of the triplet state determined as 0-0 transition was found to be located at 23 640 cm^{-1} (423 nm). This value is similar to the ones reported in the literature for the free BP[37] and BP-containing ligands (23 500–24 100 cm^{-1}).[20]

Near-infrared lanthanide(III) emission

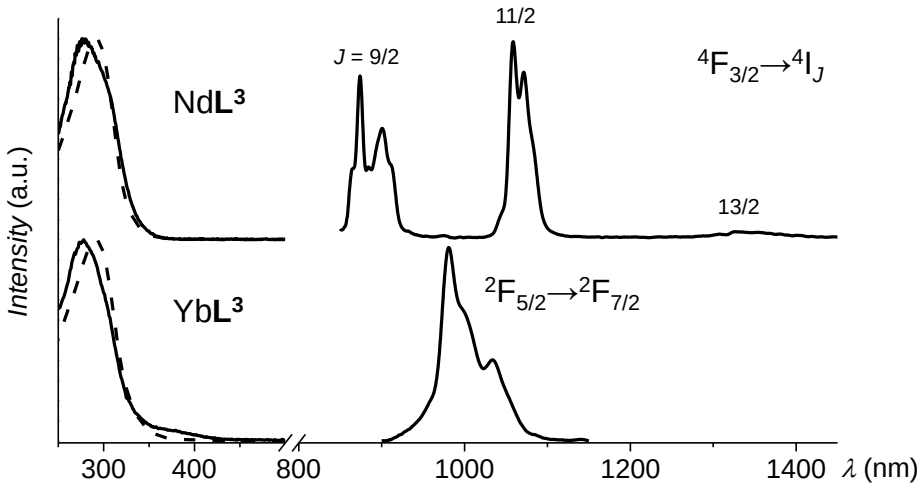

Figure 7. Corrected and normalized (left) excitation (upon monitoring the Yb^{III} sharp emission band at 980 nm for Yb**L**^{3} and monitoring one of the Nd^{III} sharp band at 1064 nm for Nd**L**^{3} (solid lines)) and superimposed absorption spectra (dashed lines), and (right) emission spectra under excitation at 300 nm of Ln**L**^{3} (Ln = Yb^{III}, Nd^{III}; 100 µM, 25 mM HEPES buffer, pH = 7.4, room temperature).

Upon excitation into ligand-centered transitions at 300 nm, Yb**L**^{3} and Nd**L**^{3} complexes in aqueous solutions exhibit characteristic sharp-band emission in the NIR range arising from the $^{2}F_{5/2} \rightarrow {}^{2}F_{7/2}$ or the $^{4}F_{3/2} \rightarrow {}^{4}I_{J}$ (J = 9/2, 11/2, 13/2) transitions, respectively (Figure 7, right). Excitation spectra of Yb**L**^{3} and Nd**L**^{3} (Figure 7, left, solid lines) collected upon monitoring their respective main transitions at 980 or 1064 nm resemble the absorption spectra (Figure 7, left, dashed lines). Such similarity confirms that characteristic Yb^{III} and Nd^{III} emission is sensitized through the "antenna effect", i.e. energy transfer from the ligand-centered energy levels. Moreover, in the excitation spectrum of Yb**L**^{3}, the band of lower intensity located at longer wavelengths (up to 420 nm) could be detected indicating that other energy levels located on the chromophore can be involved in the sensitization process of this ion. It is important to mention that in previous reports, the sensitization of Yb^{III} by the triplet state of the BP chromophore in a ternary DO3A complex with benzoylbenzoate has been reported to be negligible while an intense Nd^{III} emission could be detected.[20] Here, we established that BP chromophore in Ln**L**^{3} can serve as sensitizer for both Yb^{III} and Nd^{III} characteristic NIR emissions. Nevertheless, the values of quantum yields determined upon ligand excitation at 300 nm are 3.8-times lower for Yb**L**^{3} compared to Nd**L**^{3}, i.e. $4.9(2)\cdot10^{-3}$ *vs.* $1.84(3)\cdot10^{-2}$ %. Experimental luminescence decays are monoexponential in the case of Nd**L**^{3}

with an average value of observed lifetime equal to 92.4(5) ns. On the other hand, for Yb**L**^{3} luminescence decays are best fitted by biexponential functions with two main components with fairly different values: τ_1 = 2.28(2) µs (68%) and τ_2 = 0.69(1) µs (32%). In general, luminescence lifetimes and quantum yields of Yb**L**^{3} and Nd**L**^{3} are similar to the values reported previously for the corresponding Ln^{III} complexes formed with cyclen ligands in aqueous solutions.[38]

Following the affirmative relaxometric response of Gd**L**^{3} to zwitterionic neurotransmitters and that the characteristic NIR emission of Yb^{III} and Nd^{III} ions could be efficiently sensitized in aqueous solutions containing either Yb**L**^{3} or Nd**L**^{3} complexes, we attempted to modulate their respective NIR signals upon titration with different types of neurotransmitters. Such experiments require the repetitive monitoring of emission spectra in the NIR upon excitation of the sensitizing ligand (300 nm). Nevertheless, during the first trials, we have discovered that along with the decrease of the NIR emission signals, significant changes in the absorption spectra could be detected thus creating an ambiguity in interpreting the response of Yb**L**^{3} and Nd**L**^{3} complexes to neurotransmitters.

Indeed, in addition to its ability to sensitize luminescent lanthanides, BP is also a well-known photosensitizer at the center of many photochemical reactions: upon UV irradiation, it forms a biradical that can abstract a hydrogen atom from an available donor to form a stable hydroxyl radical (ketyl radical). The latter reacts preferentially with unreactive C-H bonds with high regio- and stereospecificity. Taking advantage of this capability, BP has been used to induce the photo-oxidative degradation of polymers[39-40] and to covalently label proteins[41-44] in order to determine conformations and to identify peptide-protein interactions or the amino acid sequence of ligand binding sites in a target protein.[45] Nevertheless, none of the few publications describing luminescent Ln^{III} complexes with BP-containing ligands[18-19, 37, 46] addressed the issue of photostability or light-induced photochemical reactions occurring in such complexes. Therefore, we have investigated the observed changes in emission and absorption spectra of Ln**L**^{3} upon illumination at 300 nm. The more detailed studies have been performed on solutions of Yb**L**^{3}. It was found that the characteristic emission of Yb^{III} in the NIR continuously decreases upon illumination reaching a limit of ~50% of the initial intensity (Figure 8, left). In parallel, absorption spectra undergo significant changes: the band at 300 nm decreases while giving rise to a band at 254 nm (Figure 8, right). Two isobestic points at 264 and 350 nm could be distinguished. Such behaviour is an indication of the change in the chemical structure of the ligand. On the other hand,

no release of free Ln^{III} ions could be observed by the colorimetric xylenol orange indicator test as an indication that the tetraaza-macrocycle cage binding the lanthanide ion maintains its structure and coordination ability.

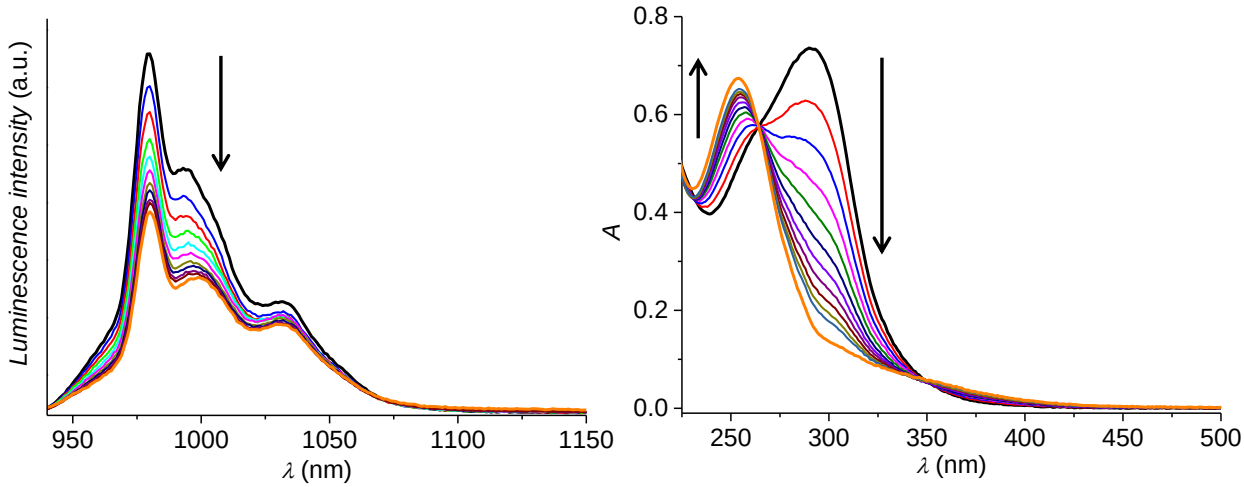

Figure 8. (Left) Emission spectra of Yb**L**^{3} upon continuous illumination at 300 nm during 40 min and (right) corresponding absorption spectra (100 μM in 25 mM HEPES buffer at pH 7.4, room temperature). Arrows indicate the direction of changes.

To monitor if the induced photochemical process is reversible or not, absorption spectra were re-measured after keeping the solution of the illuminated Yb**L**^{3} complex in the dark for 1 day. This recorded absorption spectrum was similar to the one observed immediately after illumination (Figure S5, Supporting Information), thus suggesting the irreversibility of the process. The exact identification of the species formed after illumination is a complex task and it is beyond the scope of this present study. Nevertheless, high resolution mass spectrometry studies indicated the formation of a number of species with higher molecular weights than the one of the starting complex. It should be noted also that the Yb^{III}-containing species formed after illumination of the solution of Yb**L**^{3} complex at 300 nm during 40 min exhibit a 1.35-times stronger emission intensity than the initial one which was confirmed by the comparison of the emission spectra upon excitation into isobestic points at 264 or 350 nm (Figure S6, Supporting Information).

We have studied the spectroscopic behavior of Nd**L**^{3} (Figure S7, Supporting Information) and Eu**L**^{3} (Figure S8, Supporting Information) complexes as well as of the free **L**^{3} ligand (Figure S9 Supporting Information) upon the same experimental conditions. In all cases, Ln^{III}-centered emission intensity was decreasing upon illumination while absorption spectra were undergoing

similar changes, i.e. a diminution of a band at 290 nm and the appearance of the band at shorter wavelengths. Nevertheless, the rate of the conversion (estimated from changes in absorption values *A* at 300 nm) was found to be dependent on the nature of the Ln^{III} ion. Figure 9 compares the ratio of the conversion (α) defined by the following equation:

$$\alpha = \frac{(A_0 - A_t)}{(A_t - A_f)}$$

where A_0 is the initial absorption at 300 nm and t = 0 min, A_f is the final absorption after illumination at 300 nm, assuming a full conversion. In the case of the ligand $\mathbf{L}^3$ and Yb$\mathbf{L}^3$ complex, a full conversion could be achieved after ~30 min of illumination at 300 nm, while at the same time Nd^{III} and Eu^{III} complexes demonstrated significantly slower ratios of conversion with α values of 11 and 46 %, respectively.

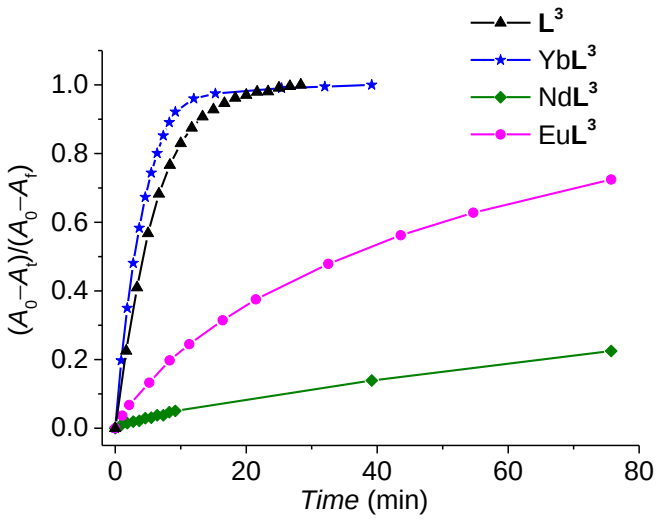

Figure 9. Conversion ratios of $\mathbf{L}^3$ and Ln$\mathbf{L}^3$ (Ln = Yb^{III}, Nd^{III}, Eu^{III}) upon continuous illumination at 300 nm (100 µM in 25 mM HEPES buffer at pH 7.4, room temperature).

As mentioned above, it is known that BP, in its triplet excited state (n,π*), can abstract hydrogen atoms from appropriate donors leading to the formation of a ketyl radical. Depending on the nature of the hydrogen donor, three main mechanisms of H-abstraction have been proposed: (i) a direct radical-like H-abstraction[47] due to the deficiency of an electron, (ii) an electron transfer followed by an H-transfer,[48] or (iii) a mechanism involving a hydrogen-bonded triplet exciplex intermediate.[49] It has been suggested also that the rate of the H-abstraction reaction is critically influenced by the hydrogen bonding interactions with the donor and its geometric orientation in

respect to the acceptor.[49] Photoreduction of BP and its derivatives by the H-abstraction process has been studied in the presence of various hydrogen-containing substrates, including aliphatic hydrocarbons, alcohols and ethers,[50-53] nucleic acids,[54-55] lipids[47] and amino acids.[56-58] These studies have been mainly conducted in non-aqueous media and the determined rate constants fall in the range 10^4 to 10^9 M^{-1} s^{-1}, while Porter has reported that protons can quench the phosphorescence of BP in aqueous solution with a rate constant of $6 \cdot 10^8$ M^{-1} s^{-1}.[59]

Based on the unambiguous changes of absorption spectra upon illumination of the **L³** ligand and Ln**L³** complexes, we can assume that an H-abstraction reaction with the BP chromophore takes place through a n,π* triplet state. Such reaction may involve, as hydrogen donor, bulk water, the buffer, or the complex itself (inter- or intramolecularly). The photochemical reaction is significantly slowered in the case of the Nd^{III}- and Eu^{III}-complexes in respect to the free ligand while for the Yb**L³** the rate of photoconversion is even slightly higher. Such behavior might be explained by different energy transfer pathways operating in the systems: (i) a dominating role of n,π* → Ln^{III} energy transfer in the case of Nd^{III}- and Eu^{III}- complexes, and (ii) an existence of an alternative sensitization pathway through an electron transfer mechanism, for example, in the case of Yb**L³**. Although the investigation of the mechanistic aspects was beyond the scope of this study, we can reasonably hypothesize that the H-abstraction reaction and the energy transfer from the triplet state to the Ln^{III} ion leading to luminescence sensitization are two competitive processes, both involving the ^{3}n,π* triplet state.

Conclusion

In summary, we have designed and synthesized a novel series of lanthanide complexes as neurotransmitter responsive probes. In order to provide optical detection capabilities in addition to MRI observation, a benzophenone was integrated in the ligand as chromophoric antenna. Relaxometric data collected upon neurotransmitter titration for the Gd^{III} complex pointed towards a decrease in the neurotransmitter-binding affinity of this probe as compared to previously described analogues that contain a benzyl instead of the benzophenone moiety. The benzophenone pendant arm enables the Gd^{3+} complex to bind to serum albumin with a high affinity. This interaction leads to increased overall relaxivity, despite a decreased hydration number of the protein conjugate. This effect in turn limits the relaxivity gain as well as neurotransmitter binding in the presence of HSA. Finally, the benzophenone provides an efficient sensitisization of the NIR

emitting Yb^{III} and Nd^{III}. This is an encouraging effect that opens possibilities for development of potent imaging probes suitable for neurotransmitter sensing by means of MR as well as optical (e.g. NIR) imaging. Nevertheless, the benzophenone concurrently exhibited another, undesired effect, i.e. a photoreaction upon long UV light exposure required for NIR detection, making the luminescence monitoring of neurotransmitters by using these complexes impossible. Importantly, the photochemical conversion rate was found to be strongly dependent on the nature of the lanthanide ion complexed giving some hints about the photophysical processes involved. Combined, this work highlights an essential set of aspects that must be considered for the development of neurotransmitter-responsive probes suitable for multimodal imaging studies, showing the great delicacy in adjusting the properties to match diverse requirements of each imaging technique.

EXPERIMENTAL SECTION

MATERIALS AND METHODS.

Preparation of the lanthanide complexes.

The synthesis of ligand **L^3** is described in the Supporting Information. Ligand **L^3** was loaded with Ln^{3+} using 0.9 equivalent of the appropriate lanthanide chloride salt ($LnCl_3 \cdot 6H_2O$) in water while the pH was kept at 6-7 during complexation. The solutions were heated at 60 °C for 1 hour to allow complete complexation. The absence of free Ln^{3+} was verified in the samples by the xylenol orange test, otherwise increments of 5% of ligand **L^3** was added until there is no free Ln^{3+} ion. The Ln^{3+} concentrations in the Ln**L** samples was determined by the bulk magnetic susceptibility method (BMS) using *tert*-butanol enriched samples.[60]

^{1}H NMRD profiles.

The $1/T_1$ NMRD profiles (1 mM; pH 7.4) were recorded at 37 and 25°C on a Stelar SMARTracer Fast Field Cycling NMR relaxometer (0.00024–0.24 T, 0.01–10 MHz ^{1}H Larmor frequency) and a Bruker WP80 NMR electromagnet adapted to variable-field measurements
(0.47–1.88 T, 20–80 MHz ^{1}H Larmor frequency) controlled by the SMARTracer PC NMR console. The temperature was controlled by a VTC91 temperature-control unit and maintained bya

gas flow, measured according to a previous calibration with a Pt resistance temperature probe. The relaxivities at 400 MHz were measured on a Bruker Avance (9.4 T) spectrometer.

^{17}O NMR spectroscopy.

Variable temperature ^{17}O NMR measurements on aqueous solution of the Gd^{3+} complexes were obtained on a on a Bruker Avance 500 (11.75 T, 67.8 MHz) spectrometer. The temperature was calculated according to a previous calibration with ethylene glycol and MeOH.[61] Acidified water ($HClO_4$, pH~4) was used as an external reference. Longitudinal ^{17}O relaxation times T_1 were measured by the inversion-recovery pulse sequence, and the transverse relaxation times (T_2) were obtained by the Carr-Purcell-Meiboom-Gill spin-echo technique. To eliminate the susceptibility corrections to the chemical shift, the samples were placed in a glass sphere fixed in a 10 mm NMR tube. The concentration of the Gd^{3+} complex was 21.4 mmol/kg (pH 6.0). To improve sensitivity, the amount of ^{17}O was enriched by adding $H_2{}^{17}O$ (10% $H_2{}^{17}O$, CortecNet) to achieve approximately 1% ^{17}O content in the sample. The least-squares fit of the data were performed by using Visualiseur/Optimiseur programs running on a MATLAB platform R2014a.[62-63]

Neurotransmitter and HSA Binding Studies.

Ternary complex formation between Gd**L**^{3} complexes and neurotransmitters was assessed by performing relaxometric titrations at 37 °C on a Bruker AvanceIII 300 MHz spectrometer. The pH was maintained at 7.4 with 25 mM HEPES buffer. A HEPES-buffered solution of the neurotransmitter was added stepwise to ~2 mM solution of Gd**L**^{3} complex solutions of up to at least 100 equivalents. Crystallized, fatty acid free and globulin free HSA was purchased from Sigma. The dissociation constants, K_d, were determined according to the following equations, where the paramagnetic relaxation rate $1/T_{1para}$ is the sum of the contributions originating from the free Gd**L** complex and the Gd**L**-analyte adduct (Gd**L**A). The $1/T_{1para}$ values measured as a function of the analyte (neurotransmitter or HSA) concentrations have been fitted to the equation below:

$$1/T_{1para} = \left(r_1^{GdLA} \times Z + (c_{GdL} - Z) \times r_1^{GdL} \right) \times 1000$$

Where

$$Z = \frac{(K_d + C_{GdL} + C_A) - \sqrt{(K_d + C_{GdL} + C_A)^2 - 4C_{A\ x}\, C_{GdL}}}{2}$$

The affinity constant is defined as:

$$K_a = \frac{1}{K_d} = \frac{[GdLA]}{[A]\times[GdL]}$$

where $r_{1\mathrm{GdL}}$ and $r_{1\mathrm{GdLA}}$ are the relaxivities of the free complex and the fully bound complex, respectively. K_a is the affinity constant, c_{GdL} and c_A represent the concentrations of GdL and of the analyte. K_a and $r_{1\mathrm{GdLA}}$ have been obtained through a two parameter fitting of the relaxation rate data measured at various analyte concentrations. Representative fits for Gd**L**^{3} are shown in Figure S10.

Photophysical measurements were performed on 100 µM HEPES-buffered solutions (25 mM) of **L^3** or Ln**L^3** complexes at pH 7.4. Absorption spectra were measured on a UVIKON XL spectrophotometer from Secomam using quartz Suprasil cells (Hellma® 115F-QS, bandpass 0.2 cm). For collecting luminescence data, samples were placed in 2.4 mm i.d. quartz capillaries or quartz Suprasil cells. Emission and excitation spectra were measured on a Horiba-Jobin-Yvon Fluorolog 3 spectrofluorimeter equipped with visible (220-800 nm, a photon-counting unit R928P) and NIR (800-1600 nm, a DSS-IGA020L Jobin-Yvon solid-state InGaAs detector cooled to 77 K, or 940-1450 nm, a photon-counting unit H10330-45 from Hamamatsu) detectors. All spectra were corrected for the instrumental functions. Luminescence lifetimes of Yb^{III} and Nd^{III} complexes were determined under excitation at 355 nm provided by a YG 980 Quantel Nd^{III}:YAG laser upon monitoring emission in the NIR range using a photon-counting unit H10330-45 from Hamamatsu. The output signal from the detector was fed into a 500 MHz bandpass digital oscilloscope (TDS 754C; Tektronix) and transferred to a PC for data processing. Luminescence lifetimes of Eu^{3+} complexes were determined under excitation at 300 nm, while the emission was monitored at 617 nm using a QuantaMasterTM 3 PH fluorescence spectrometer from Photon Technology International, Inc. (USA). Luminescence decay curves were fitted using Origin© software.

Quantum yields in the NIR were determined with a Fluorolog 3 spectrofluorimeter according to a comparative method with the Nd^{III} tropolonate as a standard (Q_{Ln}^{L} = 0.21 % in DMSO under excitation at 340 nm) using an integration sphere (Model G8, GMP SA, Renens, Switzerland). Each sample was measured several times. Estimated experimental error for quantum yields determination is ~10 %.

Determination of Ln^{III} hydration numbers from luminescence lifetimes. Luminescence lifetimes of Eu^{III} in aqueous solution and in deuterated water, τ_{H2O} and τ_{D2O}, respectively, were determined in order to estimate Eu^{III} hydration number using the following phenomenological equation:[26-27]

$$q_{Eu} = 1.2[(k_{H2O} - k_{D2O}) - 0.25 - 0.075x]$$

where $k = 1/\tau$ and x takes into account the effect of exchangeable amide N–H oscillators (assuming metal coordination of the linker amide oxygen x = 2 for Eu**L**^{3}).

Photochemical experiments were performed on 100 µM HEPES-buffered solutions (25 mM) of **L**^{3} or Ln**L**^{3} complexes at pH 7.4 at room temperature. Measurements of absorption and emission spectra were performed using quartz Suprasil cells (Hellma® 115F-QS, bandpass 0.2 cm) on a UVIKON XL spectrophotometer (Secomam) or a Horiba-Jobin-Yvon Fluorolog 3 spectrofluorimeter. Solutions in quartz cells were placed in the Fluorolog 3 spectrofluorimeter and illuminated at 300 nm (14 nm excitation slit opening) followed by corresponding mesurements.

ACKNOWLEDGMENT

The authors would also like to acknowledge the funding from the La Ligue Contre le Cancer, la Région Centre, and l'Agence Nationale de la Recherche (ANR-13-BS08-0011). S.P. acknowledges support from the Institut National de la Santé et de la Recherche Médicale (INSERM).

REFERENCES

1. Bonnet, C. S.; Tei, L.; Botta, M.; Tóth, É., Responsive Probes. In *The Chemistry of Contrast Agents in Medical Magnetic Resonance Imaging*, 2nd Edition ed.; Merbach, A. E.; Helm, L.; Tóth, É., Eds. John Wiley & Sons: Chichester, 2013; pp 343.
2. Jang, J. H.; Bhuniya, S.; Kang, J.; Yeom, A.; Hong, K. S.; Kim, J. S., Cu^{2+}-Responsive Bimodal (Optical/MRI) Contrast Agent for Cellular Imaging, *Org. Lett.* **2013,** *15*, 4702.
3. Luo, J.; Li, W.-S.; Xu, P.; Zhang, L.-Y.; Chen, Z.-N., Zn^{2+} Responsive Bimodal Magnetic Resonance Imaging and Fluorescent Imaging Probe Based on a Gadolinium(III) Complex, *Inorg. Chem.* **2012,** *51*, 9508.
4. He, J. F.; Bonnet, C. S.; Eliseeva, S. V.; Lacerda, S.; Chauvin, T.; Retailleau, P.; Szeremeta, F.; Badet, B.; Petoud, S.; Toth, E.; Durand, P., Prototypes of Lanthanide(III) Agents Responsive to Enzymatic Activities in Three Complementary Imaging Modalities: Visible/Near-Infrared Luminescence, PARACEST-, and T-1-MRI, *J. Am. Chem. Soc.* **2016,** *138*, 2913.
5. Bonnet, C. S.; Buron, F.; Caille, F.; Shade, C. M.; Drahos, B.; Pellegatti, L.; Zhang, J.; Villette, S.; Helm, L.; Pichon, C.; Suzenet, F.; Petoud, S.; Tóth, É., Pyridine-Based Lanthanide Complexes Combining MRI and NIR Luminescence Activities, *Chem. Eur. J.* **2012,** *18*, 1419.
6. Bonnet, C. S.; Tóth, É., Towards highly efficient, intelligent and bimodal imaging probes: Novel approaches provided by lanthanide coordination chemistry, *Compt. Rend. Chimie* **2010,** *13*, 700.
7. Caillé, F.; Bonnet, C. S.; Buron, F.; Villette, S.; Helm, L.; Petoud, S.; Suzenet, F.; Tóth, É., Isoquinoline-based lanthanide complexes: bright NIR optical probes and efficient MRI agents, *Inorg. Chem.* **2012,** *51*, 2522.
8. Bünzli, J. C. G., Lanthanide Luminescence for Biomedical Analyses and Imaging, *Chem. Rev.* **2010,** *110*, 2729.
9. Uh, H.; Petoud, S., Novel antennae for the sensitization of near infrared luminescent lanthanide cations, *Compt. Rend. Chimie* **2010,** *13*, 668.
10. Angelovski, G.; Tóth, É., Strategies for sensing neurotransmitters with responsive MRI contrast agents, *Chem. Soc. Rev.* **2017,** *46*, 324.
11. Lee, T.; Cai, L. X.; Lelyveld, V. S.; Hai, A.; Jasanoff, A., Molecular-Level Functional Magnetic Resonance Imaging of Dopaminergic Signaling, *Science* **2014,** *344*, 533.
12. Shapiro, M. G.; Westmeyer, G. G.; Romero, P. A.; Szablowski, J. O.; Kuster, B.; Shah, A.; Otey, C. R.; Langer, R.; Arnold, F. H.; Jasanoff, A., Directed evolution of a magnetic resonance imaging contrast agent for noninvasive imaging of dopamine, *Nature Biotech.* **2010,** *28*, 264.
13. Oukhatar, F.; Même, S.; Même, W.; Szeremeta, F.; Logothetis, N. K.; Angelovski, G.; Tóth, É., MRI sensing of neurotransmitters with a crown ether appended Gd^{3+} complex, *ACS Chem. Neurosci.* **2015,** *6*, 219.
14. Oukhatar, F.; Meudal, H.; Landon, C.; Logothetis, N. K.; Platas-Iglesias, C.; Angelovski, G.; Tóth, É., Macrocyclic Gd^{3+} complexes with pendant crown ethers designed for binding zwitterionic neurotransmitters, *Chem. Eur. J.* **2015,** *21*, 11226.
15. Pradhan, T.; Jung, H. S.; Jang, J. H.; Kim, T. W.; Kang, C.; Kim, J. S., Chemical sensing of neurotransmitters, *Chem. Soc. Rev.* **2014,** *43*, 4684.

16. Martinic, I.; Eliseeva, S. V.; Petoud, S., Near-infrared emitting probes for biological imaging: Organic fluorophores, quantum dots, fluorescent proteins, lanthanide(III) complexes and nanomaterials, *J. Luminesc.* **2017,** *189*, 19.
17. Shiraishi, Y.; Koizumi, H.; Hirai, T., Photosensitized oxygenation of sulfides within an amphiphilic dendrimer containing a benzophenone core, *J. Phys. Chem. B* **2005,** *109*, 8580.
18. Beeby, A.; Bushby, L. M.; Maffeo, D.; Williams, J. A. G., The efficient intramolecular sensitisation of terbium(III) and europium(III) by benzophenone-containing ligands, *J. Chem. Soc. Perkin Trans. 2* **2000,** 1281.
19. Wilkinson, A. J.; Maffeo, D.; Beeby, A.; Foster, C. E.; Williams, J. A. G., Sensitization of europium(III) luminescence by benzophenone-containing ligands: regioisomers, rearrangements and chelate ring size, and their influence on quantum yields, *Inorg. Chem.* **2007,** *46*, 9438.
20. Pope, S. J.; Burton-Pye, B. P.; Berridge, R.; Khan, T.; Skabara, P. J.; Faulkner, S., Self-assembly of luminescent ternary complexes between seven-coordinate lanthanide(III) complexes and chromophore bearing carboxylates and phosphonates, *Dalton Trans.* **2006,** 2907.
21. Monti, S.; Ottani, S.; Manoli, F.; Manet, I.; Scagnolari, F.; Zambelli, B.; Marconi, G., Chiral recognition of 2-(3-benzoylphenyl)propionic acid (ketoprofen) by serum albumin: an investigation with microcalorimetry, circular dichroism and molecular modelling, *Phys. Chem. Chem. Phys.* **2009,** *11*, 9104.
22. Kobayashi, H.; Longmire, M. R.; Ogawa, M.; Choyke, P. L., Rational chemical design of the next generation of molecular imaging probes based on physics and biology: mixing modalities, colors and signals, *Chem. Soc. Rev.* **2011,** *40*, 4626.
23. Torrens, A.; Mas, J.; Port, A.; Castrillo, J. A.; Sanfeliu, O.; Guitart, X.; Dordal, A.; Romero, G.; Fisas, M. A.; Sanchez, E.; Hernandez, E.; Perez, P.; Perez, R.; Buschmann, H., Synthesis of new benzoxazinone derivatives as neuropeptide Y5 antagonists for the treatment of obesity, *J. Med. Chem.* **2005,** *48*, 2080.
24. Tóth, É.; Helm, L.; Merbach, A., Relaxivity of Gadolinium(III) Complexes: Theory and Mechanism. In *The Chemistry of Contrast Agents in Medical Magnetic Resonance Imaging*, John Wiley & Sons, Ltd: 2013; pp 25.
25. Powell, D. H.; Dhubhghaill, O. M. N.; Pubanz, D.; Helm, L.; Lebedev, Y. S.; Schlaepfer, W.; Merbach, A. E., Structural and Dynamic Parameters Obtained from ^{17}O NMR, EPR, and NMRD Studies of Monomeric and Dimeric Gd^{3+} Complexes of Interest in Magnetic Resonance Imaging: An Integrated and Theoretically Self-Consistent Approach, *J. Am. Chem. Soc.* **1996,** *118*, 9333.
26. Beeby, A.; Clarkson, I. M.; Dickins, R. S.; Faulkner, S.; Parker, D.; Royle, L.; de Sousa, A. S.; Williams, J. A. G.; Woods, M., Non-radiative deactivation of the excited states of europium, terbium and ytterbium complexes by proximate energy-matched OH, NH and CH oscillators: an improved luminescence method for establishing solution hydration states, *J. Chem. Soc. Perkin Trans. 2* **1999,** 493.
27. Supkowski, R. M.; Horrocks, W. D., Jr., On the determination of the number of water molecules, q, coordinated to europium(III) ions in solution from luminescence decay lifetimes, *Inorg. Chim. Acta* **2002,** *340*, 44.
28. Graeppi, N.; Powell, D. H.; Laurenczy, G.; Zékány, L.; Merbach, A., Coordination equilibria and water exchange kinetics of lanthanide(III) propylenediaminetetraacetates and other magnetic resonance imaging related complexes, *Inorg. Chim. Acta* **1995,** *235*, 311.

29. Ruloff, R.; Tóth, É.; Scopelliti, R.; Tripier, R.; Handel, H.; Merbach, A. E., Accelerating water exchange for Gd^{III} chelates by steric compression around the water binding site, *Chem. Commun.* **2002,** 2630.
30. Aime, S.; Gianolio, E.; Longo, D.; Pagliarin, R.; Lovazzano, C.; Sisti, M., New Insights for Pursuing High Relaxivity MRI Agents from Modelling the Binding Interaction of GdIII Chelates to HSA, *ChemBioChem* **2005,** *6*, 818.
31. Fasano, M.; Curry, S.; Terreno, E.; Galliano, M.; Fanali, G.; Narciso, P.; Notari, S.; Ascenzi, P., The extraordinary ligand binding properties of human serum albumin, *IUBMB life* **2005,** *57*, 787.
32. Caravan, P., Protein-targeted gadolinium-based magnetic resonance imaging (MRI) contrast agents: design and mechanism of action, *Acc. Chem. Res.* **2009,** *42*, 851.
33. Kaneko, K.; Chuang, V. T.; Ito, T.; Suenaga, A.; Watanabe, H.; Maruyama, T.; Otagiri, M., Arginine 485 of human serum albumin interacts with the benzophenone moiety of ketoprofen in the binding pocket of subdomain III A and III B, *Pharmazie* **2012,** *67*, 414.
34. Caravan, P.; Cloutier, N. J.; Greenfield, M. T.; McDermid, S. A.; Dunham, S. U.; Bulte, J. W. M.; Amedio, J. C. J.; Looby, R. J.; Supkowski, R. M.; Horrocks, W. D. J.; McMurry, T. J.; B., L., The Interaction of MS-325 with Human Serum Albumin and Its Effect on Proton Relaxation Rates, *J. Am. Chem. Soc.* **2002,** *124*, 3152.
35. Zech, S. G.; Sun, W. C.; Jacques, V.; Caravan, P.; Astashkin, A. V.; Raitsimring, A. M., Probing the Water Coordination of Protein-Targeted MRI Contrast Agents by Pulsed ENDOR Spectroscopy, *ChemPhysChem* **2005,** *6*, 2570.
36. Skvortsova, V. I.; Raevskii, K. S.; Kovalenko, A. V.; Kudrin, V. S.; Malikova, L. A.; Sokolov, M. A.; Alekseev, A. A.; Gusev, E. I., Levels of neurotransmitter amino acids in the cerebrospinal fluid of patients with acute ischemic insult, *Neuroscience and behavioral physiology* **2000,** *30*, 491.
37. Shiraishi, Y.; Furubayashi, Y.; Nishimura, G.; Hirai, T., Sensitized luminescence properties of dinuclear lanthanide macrocyclic complexes bearing a benzophenone antenna, *J. Luminesc.* **2007,** *127*, 623.
38. Mewis, R. E.; Archibald, S. J., Biomedical applications of macrocyclic ligand complexes, *Coord. Chem. Rev.* **2010,** *254*, 1686.
39. Lin, C. S.; Liu, W. L.; Chiu, Y. S.; Ho, S.-Y., Benzophenone-sensitized photodegradation of polystyrene films under atmospheric conditions, *Polym. Degr. Stability* **1992,** *38*, 125.
40. Harper, D. J.; McKellar, J. F., Mechanism of the benzophenone-sensitized photodegradation of polypropylene, *J. Appl. Pol. Sci.* **1973,** *17*, 3503.
41. Chuang, V. T.; Otagiri, M., Photoaffinity labeling of plasma proteins, *Molecules* **2013,** *18*, 13831.
42. Dorman, G.; Prestwich, G. D., Benzophenone photophores in biochemistry, *Biochemistry* **1994,** *33*, 5661.
43. Prestwich, G. D.; Dorman, G.; Elliott, J. T.; Marecak, D. M.; Chaudhary, A., Benzophenone photoprobes for phosphoinositides, peptides and drugs, *Photochem. Photobiol.* **1997,** *65*, 222.
44. Chuang, V. T. G.; Kuniyasu, A.; Nakayama, H.; Matsushita, Y.; Hirono, S.; Otagiri, M., Helix 6 of subdomain III A of human serum albumin is the region primarily photolabeled by ketoprofen, an arylpropionic acid NSAID containing a benzophenone moiety, *Biochim. Biophys Acta - Protein Structure and Molecular Enzymology* **1999,** *1434*, 18.

45. Dormán, G.; Prestwich, G. D., Using photolabile ligands in drug discovery and development, *Trends in Biotechn.* **2000,** *18*, 64.
46. Shiraishi, Y.; Furubayashi, Y.; Nishimura, G.; Hirai, T., Sensitized luminescence of Eu and Tb macrocyclic complexes bearing benzophenone antennae, *J. Luminesc.* **2007,** *126*, 68.
47. Markovic, D. Z.; Patterson, L. K., Radical Processes in Lipids. Selectivity of Hydrogen Abtraction from Lipids by Benzophenone Triplet, *Photochem. Photobiol.* **1989,** *49*, 531.
48. Cohen, S. G.; Cohen, J. I., Photoreduction of p-Aminobenzophenone. Effect of Tertiary Amines, *J. Am. Chem. Soc.* **1967,** *89*, 164.
49. Leigh, W. J.; Lathioor, E. C.; St. Pierre, M. J., Photoinduced Hydrogen Abstraction from Phenols by Aromatic Ketones. A New Mechanism for Hydrogen Abstraction by Carbonyl n,π* and π,π* Triplets, *Journal of the American Chemical Society* **1996,** *118*, 12339.
50. H Mallesha, N. D. D., K S Rangappa, S Shashikanth, N K Lokanath, M A Sridhar & J Shashidhara Prasad, Photoreduction of benzophenone analogues by alcohol and ether: Self recognition molecular assemblies, *Ind. J. Chem. B* **2002,** *41*, 196.
51. Beckett, A.; Porter, G., Primary photochemical processes in aromatic molecules. Part 9.-Photochemistry of benzophenone in solution, *Trans. of the Faraday Society* **1963,** *59*, 2038.
52. Demeter, A.; László, B.; Bérces, T., Kinetics of Ketyl Radical Reactions Occurring in the Photoreduction of Benzophenone by Isopropyl Alcohol, *Bericht. Bunsengesell. Phys. Chem.* **1988,** *92*, 1478.
53. Demeter, A.; Horváth, K.; Böőr, K.; Molnár, L.; Soós, T.; Lendvay, G., Substituent Effect on the Photoreduction Kinetics of Benzophenone, *J. Phys. Chem. A* **2013,** *117*, 10196.
54. Marazzi, M.; Wibowo, M.; Gattuso, H.; Dumont, E.; Roca-Sanjuan, D.; Monari, A., Hydrogen abstraction by photoexcited benzophenone: consequences for DNA photosensitization, *Phys. Chem. Chem. Phys.* **2016,** *18*, 7829.
55. Helene, C., Phosphorescence of Benzophenone in Aqueous Solution and Its Quenching by Nucleic Acid Derivatives, *Photochem. Photobiol.* **1972,** *16*, 519.
56. Saprygina, N. N.; Morozova, O. B.; Grampp, G.; Yurkovskaya, A. V., Effect of Amino Group Charge on the Photooxidation Kinetics of Aromatic Amino Acids, *J. Phys. Chem. A* **2014,** *118*, 339.
57. Battacharyya, S. N.; Das, P. K., Photoreduction of benzophenone by amino acids, aminopolycarboxylic acids and their metal complexes. A laser-flash-photolysis study, *J. Chem. Soc. Faraday Trans. 2* **1984,** *80*, 1107.
58. Encinas, M. V.; Lissi, E. A.; Olea, A. F., Quenching of Triplet Benzophenone by Vitamins E and C and by Sulfur Containing Amino Acids and Peptides, *Photochem. Photobiol.* **1985,** *42*, 347.
59. Ledger, M. B.; Porter, G., Primary photochemical processes in aromatic molecules. Part 15.-The photochemistry of aromatic carbonyl compounds in aqueous solution, *J. Chem. Soc. Faraday Trans. 1* **1972,** *68*, 539.
60. Delaglio, F.; Grzesiek, S.; Vuister, G. W.; Zhu, G.; Pfeifer, J.; Bax, A., NMRPIPE - A Multidimensional Spectral Processing System Based on UNIX Pipes, *J. Biomol. NMR* **1995,** *6*, 277.
61. Raiford, D. S.; Fisk, C. L.; Becker, E. D., Calibration of Methanol and Ethylene Glycol Nuclear Magnetic Resonance Thermometers, *Analytical Chemistry* **1979,** *51*, 2050.
62. Yerly, F., Visualiseur 2.3.8. Institut de Chimie Moléculaire et Biologique, EPFL-BCH. Lausanne

63. Yerly, F., Optimiseur 3.0.1. Institut de Chimie Moléculaire et Biologique, EPFL-BCH. Lausanne

For Table of Contents

Macrocyclic lanthanide complexes incorporating a benzophenone chromophore and a crown ether have been assessed as neurotransmitter-responsive probes in magnetic resonance or NIR optical imaging. The binding of amino acid neurotransmitters results in a relaxivity decrease for the Gd^{3+} chelate; however, an undesired photoreaction of the benzophenone upon long UV light exposure, required for NIR detection, prevents luminescence monitoring of neurotransmitters with these complexes.